Supporting Information

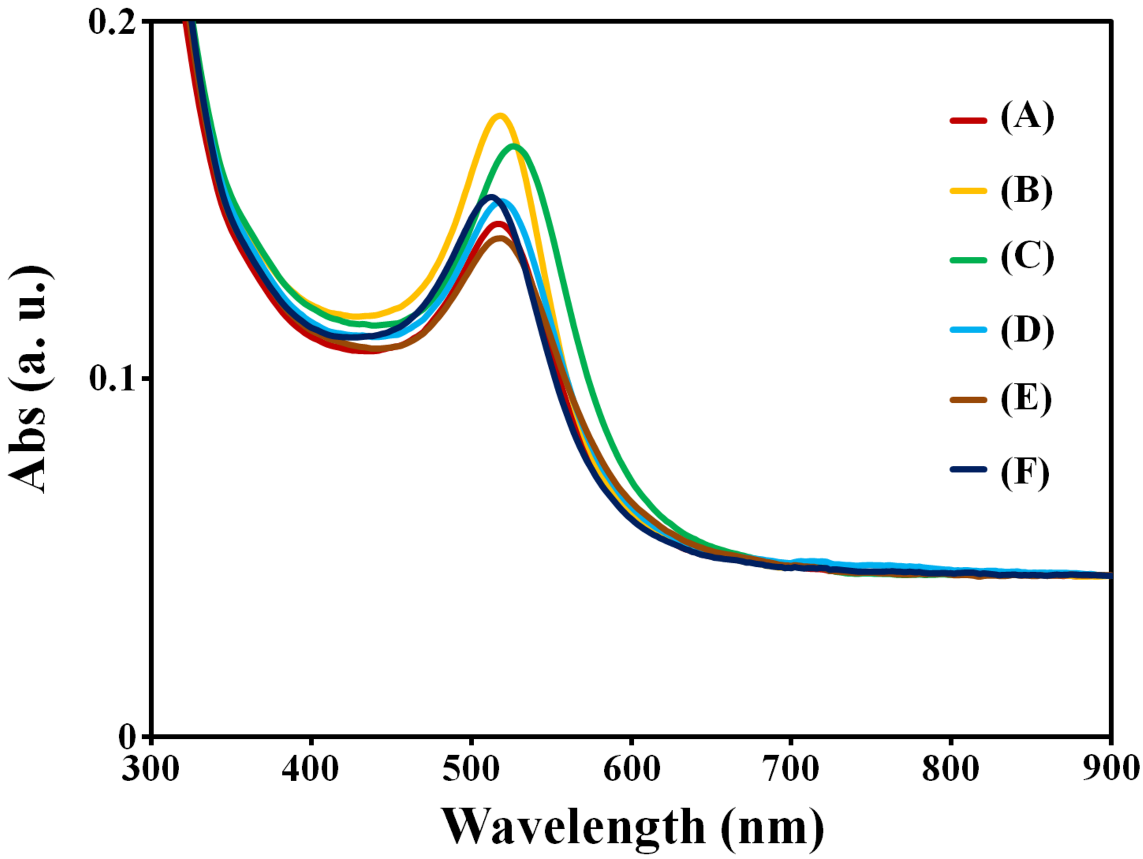

Fig. S1 UV–Vis absorbance spectra of 5.0 mM Tris-borate (pH 7.0) containing Au NPs (750 pM) in the (A) absence and (B–F) presence of (B) Ag^{+} (10 μM), (C) Bi^{3+} (10 μM), (D) Pb^{2+} 10 μM), (E) Pt^{4+} (10 μM), and (F) Hg^{2+} (10 μM).

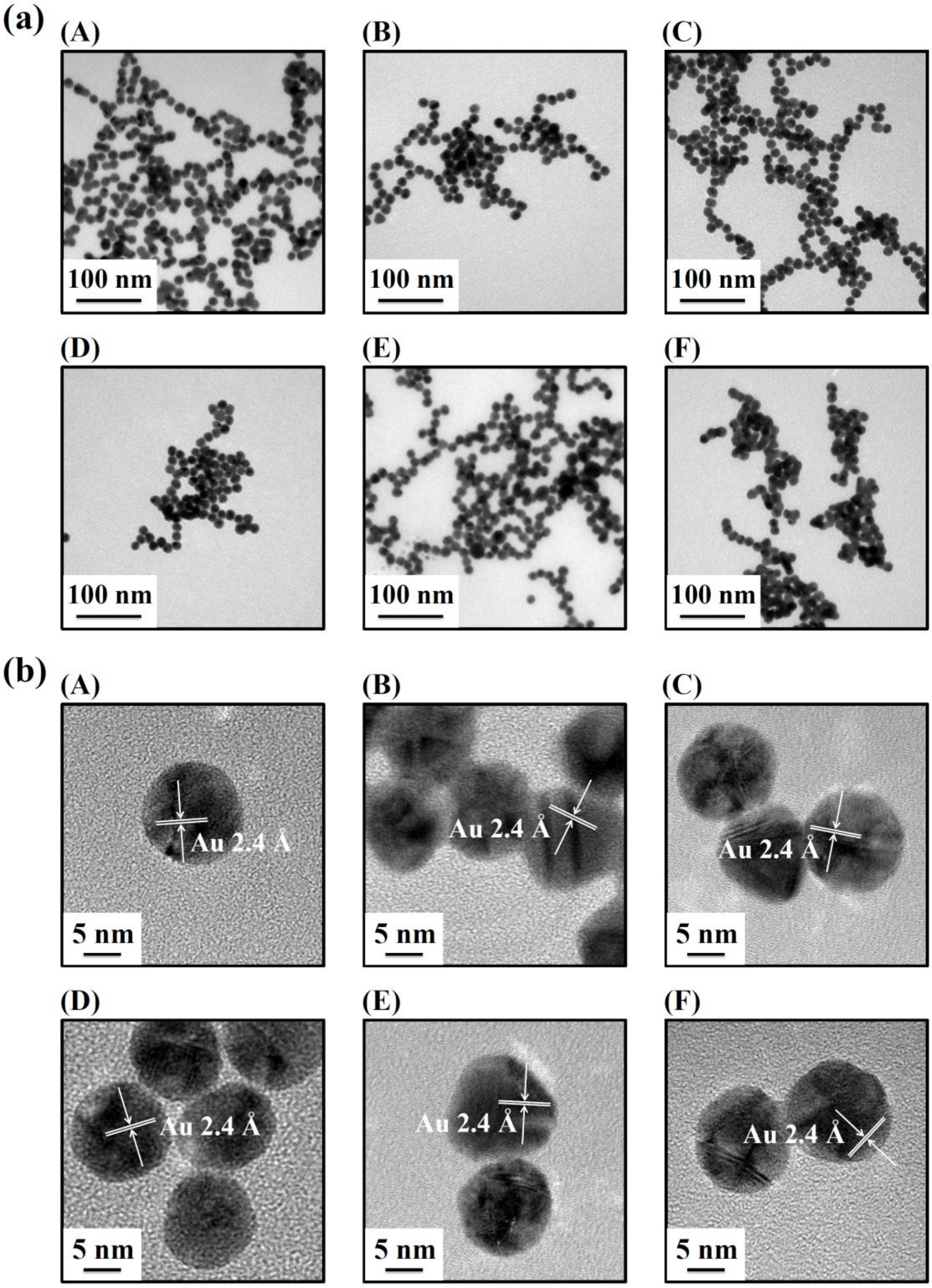

Fig. S2 (a) TEM and (b) HRTEM images of Au NPs in the (A) absence and (B–F) presence of (B) Ag^{+}, (C) Bi^{3+}, (D) Pb^{2+}, (E) Pt^{4+}, and (F) Hg^{2+}. Other conditions were the same as those described in Fig. S1. Average Au NP sizes in (a) (A–F) are 13.4 ± 1.2, 13.8 ± 1.0, 13.4 ± 1.2, 13.4 ± 1.1, 13.4 ± 1.9, and 13.3 ± 1.7 nm, respectively. The lattice fringes in (A–F) are consistent with metallic Au having a discerned lattice spacing of 2.4 Å, corresponding to the *d*-spacing of the (111) crystal plane of face-centered cubic (fcc) Au.

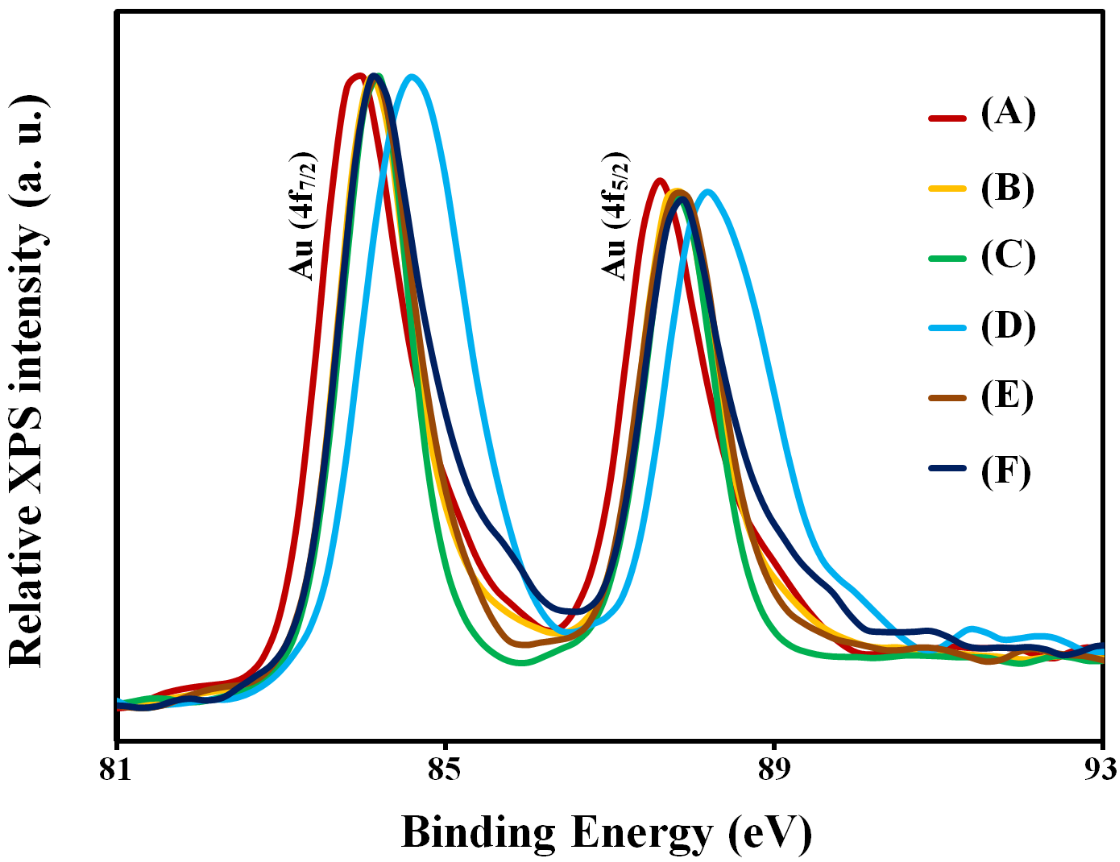

Fig. S3 Au 4f core-level photoelectron spectra of Au NPs (750 pM) in the (A) absence and (B−F) presence of (B) Ag^{+} (10 μM), (C) Bi^{3+} (10 μM), (D) Pb^{2+} (10 μM), (E) Pt^{4+} (10 μM), and (F) Hg^{2+} (10 μM) ions, dosed onto Si substrates, and measured at room temperature. Other conditions were the same as those described in Fig. S1. The binding energy (BE, 285.3 eV) of the alkyl chain C 1s orbital is given as an internal reference.

Electronic Supplementary Material (ESI) for Nanoscale

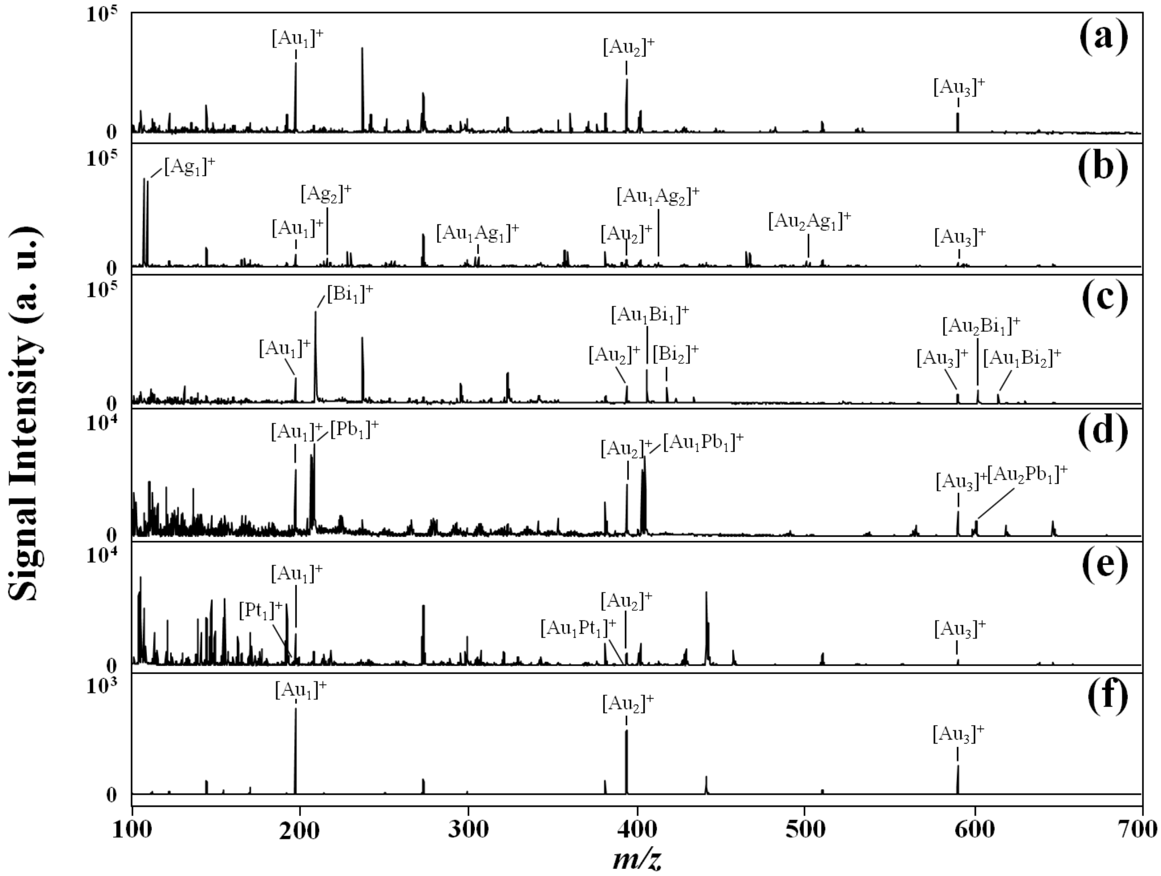

Fig. S4 SALDI mass spectra of 5.0 mM Tris-borate (pH 7.0) containing Au NPs (750 pM) in the (a) absence and (b–f) presence of (b) Ag^+ (10 μM), (c) Bi^{3+} (10 μM), (d) Pb^{2+} (10 μM), (e) Pt^{4+} (10 μM), and (f) Hg^{2+} (10 μM) ions. The peaks in (a) at *m/z* 196.97, 393.93, and 590.90 are assigned to $[Au_1]^+$, $[Au_2]^+$, and $[Au_3]^+$ ions, respectively. The peaks in (b) at *m/z* 106.90, 108.90, 213.81, 215.81, 217.81, 303.87, 305.87, 410.78, 412.78, 414.78, 500.84, and 502.84 are assigned to $[^{106.90}Ag]^+$, $[^{108.90}Ag]^+$, $[^{106.90}Ag + {}^{106.90}Ag]^+$, $[^{106.90}Ag + {}^{108.90}Ag]^+$, $[^{108.90}Ag + {}^{108.90}Ag]^+$, $[Au_1 + {}^{106.90}Ag]^+$, $[Au_1 + {}^{108.90}Ag]^+$, $[Au_1 + {}^{106.90}Ag + {}^{106.90}Ag]^+$, $[Au_1 + {}^{106.90}Ag + {}^{108.90}Ag]^+$, $[Au_1 + {}^{108.90}Ag + {}^{108.90}Ag]^+$, $[Au_2 + {}^{106.90}Ag]^+$, and $[Au_2 + {}^{108.90}Ag]^+$ ions, respectively. The peaks in (c) at *m/z* 208.98, 405.95, 417.96, 602.91, and 614.93 are assigned to $[Bi_1]^+$, $[Au_1Bi_1]^+$, $[Bi_2]^+$, $[Au_2Bi_1]^+$, and $[Au_1Bi_2]^+$ ions, respectively. The peaks in (d) at *m/z* 205.97, 206.98, 207.98, 402.94, 403.94, 404.94, 599.91, 600.91, and 601.91 are assigned to $[^{205.97}Pb]^+$, $[^{206.98}Pb]^+$, $[^{207.98}Pb]^+$, $[Au_1 + {}^{205.97}Pb]^+$, $[Au_1 + {}^{206.98}Pb]^+$, $[Au_1 + {}^{207.98}Pb]^+$, $[Au_2 + {}^{205.97}Pb]^+$, $[Au_2 + {}^{206.98}Pb]^+$, and $[Au_2 + {}^{207.98}Pb]^+$ ions, respectively. The peaks in (e) at *m/z* 193.96, 194.96, 195.96, 390.93, 391.93, and 392.93 are assigned to $[^{193.96}Pt]^+$, $[^{194.96}Pt]^+$, $[^{195.96}Pt]^+$, $[Au_1 + {}^{193.96}Pt]^+$, $[Au_1 + {}^{194.96}Pt]^+$, and $[Au_1 + {}^{195.96}Pt]^+$ ions, respectively. Other conditions were the same as those described in Fig. S1. A total of 500 pulsed laser shots were applied under a laser fluence set at 51.25 μJ.

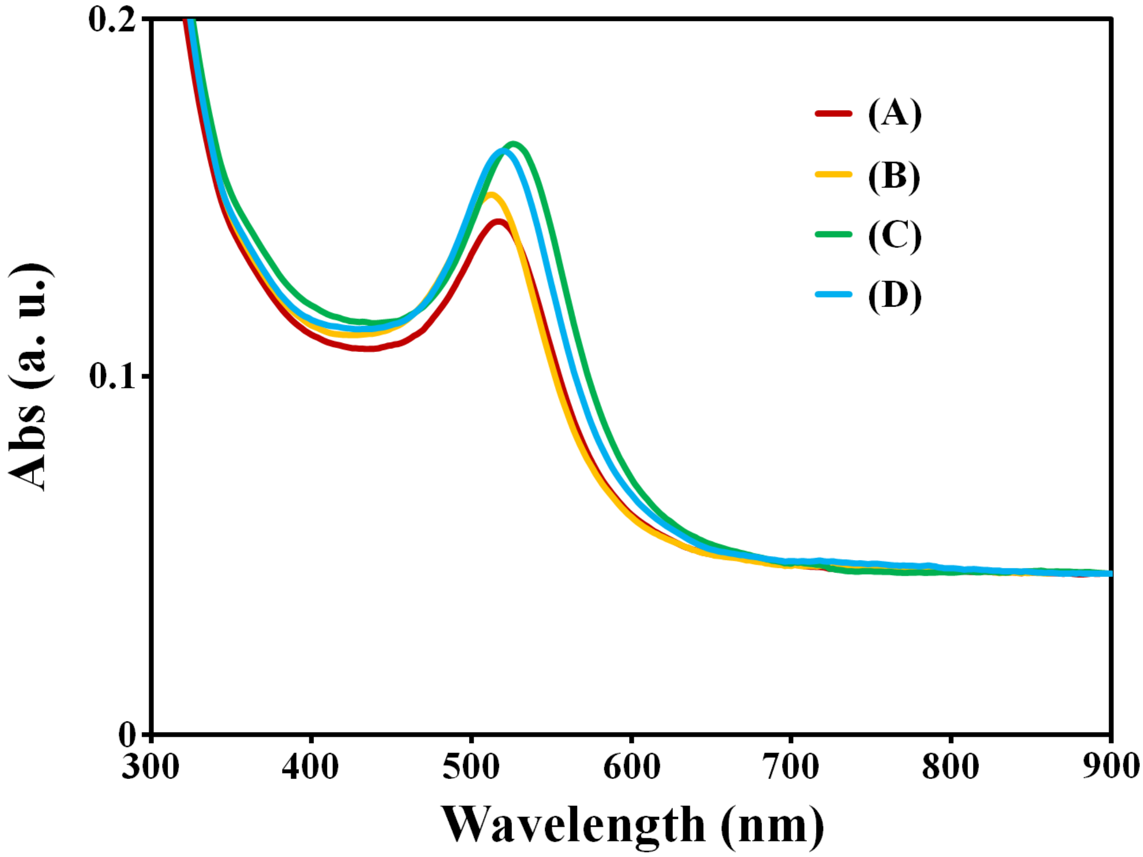

Fig. S5 UV–Vis absorbance spectra of 5.0 mM Tris-borate (pH 7.0) containing Au NPs (750 pM) in the (A) absence and (B–D) presence of (B) Hg^{2+} (10 μM), (C) Bi^{3+} (10 μM), and (D) Hg^{2+} (10 μM) and Bi^{3+} (10 μM) ions. Other conditions were the same as those described in Fig. S1.

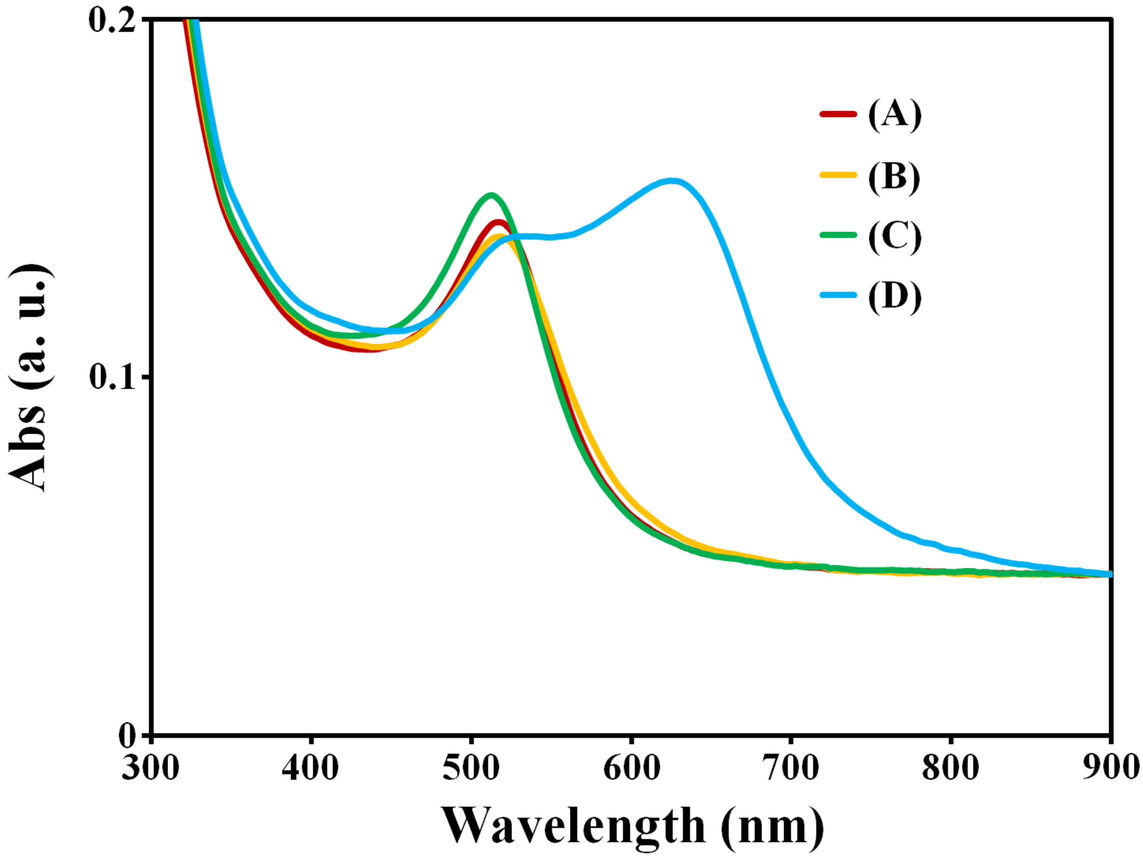

Fig. S6 UV–Vis absorbance spectra of 5.0 mM Tris-borate (pH 7.0) containing Au NPs (750 pM) in the (A) absence and (B–D) presence of (B) Pt^{4+} (10 μM), (C) Hg^{2+} (10 μM), and (D) Pt^{4+} (10 μM) and Hg^{2+} (10 μM) ions. Other conditions were the same as those described in Fig. S1.

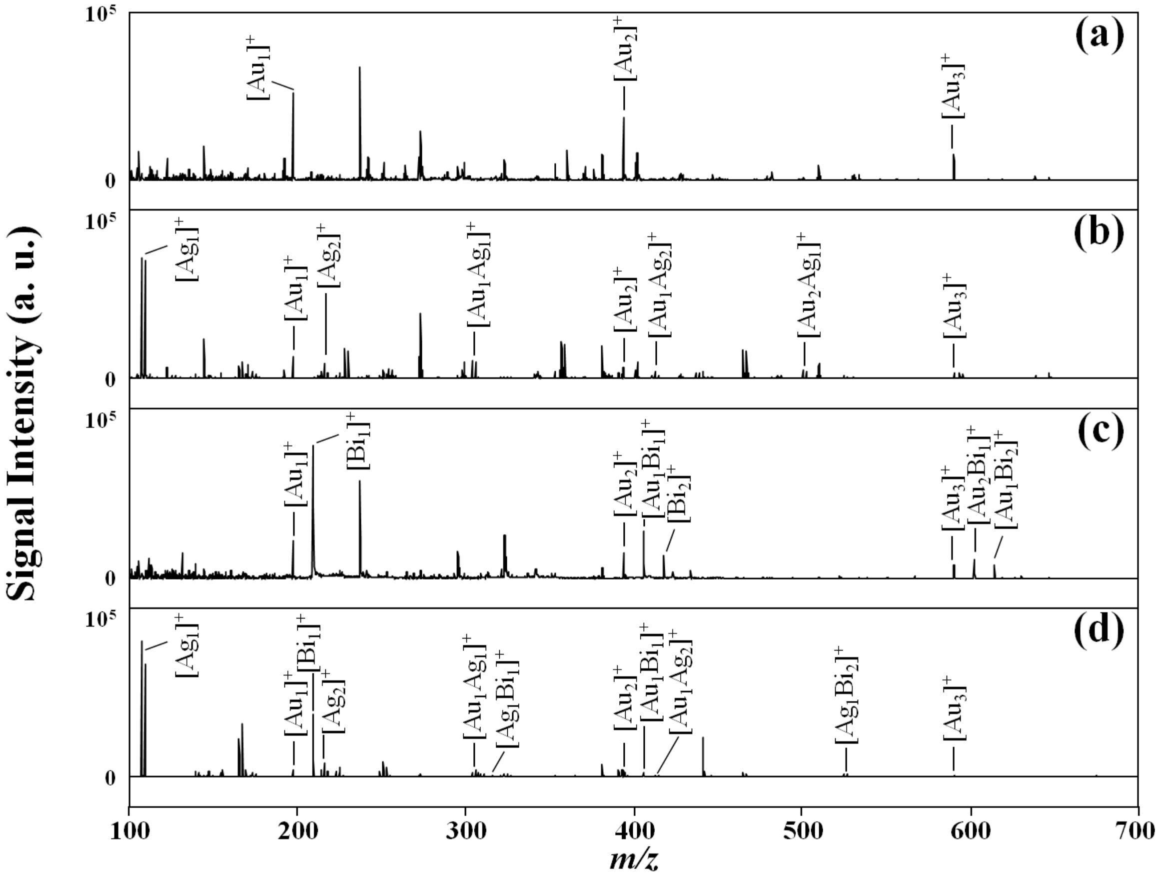

Fig. S7 SALDI mass spectra of 5.0 mM Tris-borate (pH 7.0) containing Au NPs (750 pM) in the (a) absence and (b–d) presence of (b) Ag^+ (10 μM), (c) Bi^{3+} (10 μM), and (d) Ag^+ (10 μM) and Bi^{3+} (10 μM) ions. The peaks in (a) at *m*/*z* 196.97, 393.93, and 590.90 are assigned to $[Au_1]^+$, $[Au_2]^+$, and $[Au_3]^+$ ions, respectively. The peaks in (b) at *m*/*z* 106.90, 108.90, 213.81, 215.81, 217.81, 303.87, 305.87, 410.78, 412.78, 414.78, 500.84, and 502.84 are assigned to $[^{106.90}Ag]^+$, $[^{108.90}Ag]^+$, $[^{106.90}Ag + {}^{106.90}Ag]^+$, $[^{106.90}Ag + {}^{108.90}Ag]^+$, $[^{108.90}Ag + {}^{108.90}Ag]^+$, $[Au_1 + {}^{106.90}Ag]^+$, $[Au_1 + {}^{108.90}Ag]^+$, $[Au_1 + {}^{106.90}Ag + {}^{106.90}Ag]^+$, $[Au_1 + {}^{106.90}Ag + {}^{108.90}Ag]^+$, $[Au_1 + {}^{108.90}Ag + {}^{108.90}Ag]^+$, $[Au_2 + {}^{106.90}Ag]^+$, and $[Au_2 + {}^{108.90}Ag]^+$ ions, respectively. The peaks in (c) at *m*/*z* 208.98, 405.95, 417.96, 602.91, and 614.93 are assigned to $[Bi_1]^+$, $[Au_1Bi_1]^+$, $[Bi_2]^+$, $[Au_2Bi_1]^+$, and $[Au_1Bi_2]^+$ ions, respectively. The peaks in (d) at *m*/*z* 315.88, 317.88, 524.87, and 526.87 are assigned to $[^{106.90}Ag + Bi_1]^+$, $[^{108.90}Ag + Bi]^+$, $[^{106.90}Ag + Bi_2]^+$, and $[^{106.90}Ag + Bi_2]^+$ ions, respectively. Other conditions were the same as those described in Fig. S1. A total of 500 pulsed laser shots were applied under a laser fluence set at 51.25 μJ.